

Triple Junction at the Triple Point Resolved on the Individual Particle Level

M. Chaudhuri,^{1,2,3} E. Allahyarov,^{3,4} H. Löwen,³ S. U. Egelhaaf,^{5,*} and D. A. Weitz^{1,2}

¹*Department of Physics, Harvard University, Cambridge, Massachusetts 02138, USA*

²*School of Engineering and Applied Sciences, Harvard University, Cambridge, Massachusetts 02138, USA*

³*Institute for Theoretical Physics II: Soft Matter, Heinrich Heine University, 40225 Düsseldorf, Germany*

⁴*Theoretical Department, Joint Institute for High Temperatures, Russian Academy of Sciences (ITAN), Moscow 125412, Russia*

⁵*Condensed Matter Physics Laboratory, Heinrich Heine University, 40225 Düsseldorf, Germany*

(Received 11 May 2017; published 21 September 2017)

At the triple point of a repulsive screened Coulomb system, a fcc crystal, a bcc crystal, and a fluid phase coexist. At their intersection, these three phases form a liquid groove, the triple junction. Using confocal microscopy, we resolve the triple junction on a single-particle level in a model system of charged PMMA colloids in a nonpolar solvent. The groove is found to be extremely deep and the incommensurate solid-solid interface to be very broad. Thermal fluctuations hence appear to dominate the solid-solid interface. This indicates a very low interfacial energy. The fcc-bcc interfacial energy is quantitatively determined based on Young's equation and, indeed, it is only about 1.3 times higher than the fcc-fluid interfacial energy close to the triple point.

DOI: 10.1103/PhysRevLett.119.128001

According to the traditional Gibbs phase rule of thermodynamics [1], in a one-component system up to three phases can coexist. Their coexistence is represented by a triple point in the temperature-pressure phase diagram and a triple line in the temperature-density phase diagram. At triple conditions, the three phases are in mutual mechanical, thermal, and chemical equilibrium. The three possible interfaces only occur at the same time if the interfacial energies are similar; if an interfacial energy is larger than the sum of the other two, this interface is unstable and the third phase intervenes. When the three interfaces intersect, they form an interfacial line, the triple junction line (which is a point in the slice shown in Fig. 1). Triple junctions have been studied on the macroscopic level, for example, in metals where liquid lenses form on top of a crystallite surrounded by coexisting vapor [2,3]. Another classical example is the triple point of water where vapor, liquid water, and ice coexist. Such a gas-liquid-solid triple point involves two disordered and one ordered phase and can exist in systems governed by sufficiently long-ranged attractive interparticle interactions [4–6]. In contrast, the coexistence of a fluid and two different solids involves two ordered structures and hence an interface between two crystallites that are not commensurate. The corresponding phase behavior has been studied in suspensions of charged colloids [7–16], star polymers [17], microgels [18], and dusty plasmas [8,19–23]. In these systems, a fcc crystal, a bcc crystal, and a fluid can coexist. Colloids have long been used as model systems to explore such situations, including nucleation [24–27], crystallization [28–32], melting [16,33,34], defects [35], glass transition [36–39], solid-liquid interfaces [40–44], solid-solid phase transformations [45–48], as well as the microscopic response to external forces [49–52].

Using charged colloids [53,54], we investigate the triple junction at the triple point on an individual-particle level, i.e., including the smallest relevant length scale. At the triple point, we find a deep and tight fluid groove between the two solid phases and a very broad solid-solid interface. This indicates a small solid-solid interfacial energy and hence a considerable effect of thermal fluctuations. Indeed, a quantitative determination of the interfacial energy using Young's equation confirms this suggestion.

The interactions of highly charged colloids in the presence of small ions can be described by a purely repulsive screened Coulomb (or Yukawa) effective pair interaction $U(r) = (Q^2/4\pi\epsilon\epsilon_0 r) \exp(-r/\lambda)$, with the particle charge $Q = Ze$, the elementary charge e , the permittivity of the vacuum ϵ_0 , the relative permittivity ϵ , and the Debye screening length λ [11–13]. Phase space is completely parametrized by the Coulomb coupling parameter $\Gamma = Q^2/(4\pi\epsilon\epsilon_0 a k_B T) = Z^2 \lambda_B/a$ and the screening

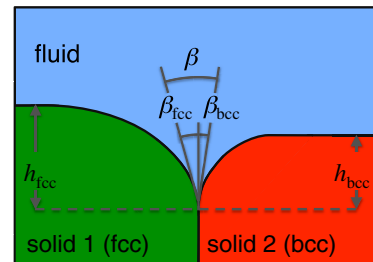


FIG. 1. Schematic representation of a triple junction involving two different solids, a fcc (green) and a bcc (red) phase, as well as a fluid (blue). A fluid groove can exist with a triple junction at its tip. The dihedral angle at the tip $\beta = \beta_{fcc} + \beta_{bcc}$ where β_{fcc} and β_{bcc} are indicated. The depths of the groove, h_{fcc} and h_{bcc} , are also indicated.

parameter $\kappa = a/\lambda$, where $k_B T$ is the thermal energy, $\lambda_B = e^2/(4\pi\epsilon\epsilon_0 k_B T)$ the Bjerrum length, $a = \rho^{-1/3}$ the mean interparticle distance, and ρ the particle number density. For this system, using molecular dynamics simulations the triple point was located at $\Gamma \approx 3500$ and $\kappa = 6.90$ [13].

We use charged fluorescently labeled PMMA spheres coated with polyhydroxystearic acid with a radius $R \approx 0.80 \mu\text{m}$, as determined by dynamic light scattering. They are suspended in a nonpolar solvent mixture of decalin ($\epsilon = 2.1$, density $\rho = 0.881 \text{ g/ml}$, refractive index $n = 1.48$) and tetrachloroethylene ($\epsilon = 2.5$, $\rho = 1.623 \text{ g/ml}$, $n = 1.51$), with a ratio of 6:5 (by volume). This mixture has a viscosity $\eta \approx 1.29 \text{ mPa s}$ as determined by rheology, a relative permittivity $\epsilon \approx 2.3$, a density that closely matches the particle density, and a refractive index very similar to the one of the particles.

In nonpolar solvents charges do not readily dissociate. However, they can be stabilized in the cores of reverse surfactant micelles [55]. They favor the dissociation of charges from the particle surface resulting in negatively charged particles and charge screening by the charged reverse micelles, similar to the mechanism in polar solvents. Furthermore, two neutral micelles can reversibly interact to yield two oppositely charged micelles; roughly 1 in 10^5 micelles acquires a single elementary charge in this way [55]. We use 20 mM dioctyl sodium sulfosuccinate (AOT), which is well above the estimated critical micelle concentration of about 1 mM [55–57], and yields reverse micelles with an essentially concentration-independent radius $R_m \approx 1.5 \text{ nm}$ [55,58]. At this AOT concentration the conductivity $c \approx 80 \text{ pS/cm}$, as measured using an immersion probe, and thus the number density of charged micelles, and hence ions, is estimated to be $\rho_m = 6\pi\eta R_m c/e^2 \approx 10^{19} \text{ m}^{-3}$ (and the number density of all, that is charged and uncharged, micelles is higher by a factor of about 10^5). This results in an estimate of the screening length $\lambda = 1/\sqrt{4\pi\lambda_B\rho_m} \approx 0.5 \mu\text{m}$, with $\lambda_B \approx 24 \text{ nm}$. Electrophoretic light scattering measurements yield the normalized zeta potential $|e\zeta/k_B T| \approx 3.6$. The particle charge number can be estimated within the Derjaguin-Landau-Verwey-Overbeek theory, $|Z| = [e^{R/\lambda}/(1 + R/\lambda)]|e\zeta/k_B T| \approx 900$ [59]. Because of charge saturation, this is only a crude upper estimate [60].

We use a sample at the triple point to determine the particle charge with high accuracy. A concentrated sample is prepared and less dense samples obtained by adding supernatant. The sample with three coexisting phases is identified using confocal microscopy [61]. The three coexisting phases have slightly different particle number densities, $\rho \approx 0.030 \mu\text{m}^{-3}$ (fluid), $0.035 \mu\text{m}^{-3}$ (bcc), and $0.040 \mu\text{m}^{-3}$ (fcc) (Fig. 2, filled stars), which is consistent with the small size of the coexistence region predicted for highly charged particles [11]. At the triple point, $\Gamma \approx 3500$ and $\kappa = 6.90$ [13]. This suggests a screening length $\lambda \approx 0.45 \mu\text{m}$ consistent with the estimated $\lambda \approx 0.5 \mu\text{m}$ and a particle charge $|Q| \approx 670e$, which is below the crude upper

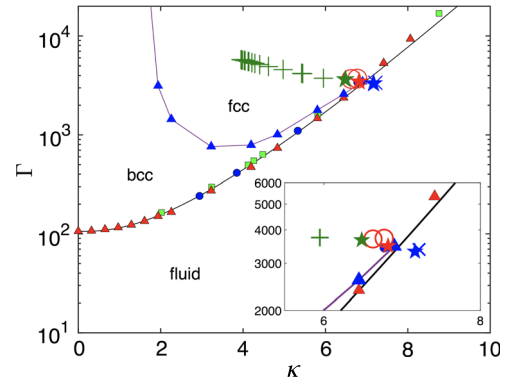


FIG. 2. Phase diagram of the purely repulsive Yukawa system as a function of the Coulomb coupling parameter Γ and the screening parameter κ . The experimentally investigated samples in the different single-phase regions are represented by + (fcc), \circ (bcc), and \times (fluid), and the three coexisting phases in the sample under triple conditions by green stars (fcc), red stars (bcc), and blue stars (fluid). The theoretically predicted fluid-solid coexistence line is indicated by red triangles [13], blue solid circles [14], and green squares [15], and the corresponding analytical expression $\Gamma = 106e^\kappa/(1 + \kappa + 0.5\kappa^2)$ [23] by a solid line. The theoretically predicted fcc-bcc coexistence is indicated by blue triangles connected by a line. The inset shows the data close to the triple point.

estimate $|Q| \approx 900e$. Thus, the values determined from the sample at the triple point are consistent with those based on the sample composition. It also confirms that the particles are highly charged. This can be quantified by the reduced contact value of the pair potential consisting of repulsive Yukawa and hard core interactions, $\Gamma^* = Z^2(\lambda_B/2R)(1 + R/\lambda)^{-2} \approx 900$ [8,11]. Thus, $\Gamma^* \gg 20$ and hard core interactions are negligible [11]. The particles hence can be treated as highly charged, pointlike particles with purely repulsive screened Coulomb interactions.

Having determined the particle charge $Q \approx -670e$ and the screening length $\lambda \approx 0.45 \mu\text{m}$, using these parameters we can locate the samples in the phase diagram (Fig. 2). The observed phase behavior is consistent with previous experimental findings and theoretical predictions for a repulsive screened Coulomb system [9–15,23,62–67].

The sample with three coexisting phases is investigated in more detail in the following. Confocal microscopy images taken $20 \mu\text{m}$ from the cover slip show the coexistence of two crystalline solids and a fluid (Fig. 3) and thus fluid-solid interfaces as well as a solid-solid interface. At the solid-solid-fluid triple line a fluid groove starts that is many crystal layers deep. It has a small dihedral angle that appears slightly asymmetric, reflecting the two different crystalline solids. This is different in grain-boundary grooves that are formed between crystallites of the same structure, which have experimentally been observed in hard sphere systems [48,68].

Images of the groove are quantitatively analyzed to retrieve a profile of the groove and to determine the crystal

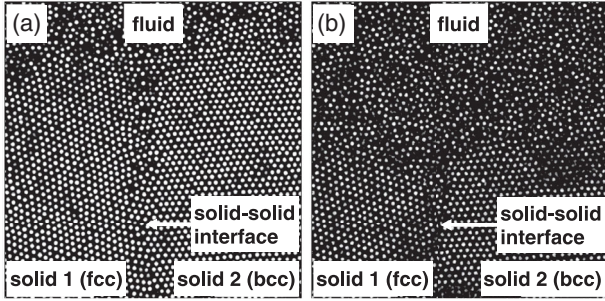


FIG. 3. Coexistence of two crystalline solids and one fluid as observed by confocal microscopy in the sample under triple conditions. From the three-dimensional stack of images, the two outermost slices, which are (a) $20 \mu\text{m}$ and (b) $80 \mu\text{m}$ from the cover slip, respectively, are shown. The slices are $145 \times 145 \mu\text{m}^2$.

structures. This requires us to determine whether a particle belongs to the fluid or one of the solids. The particle locations are extracted from the image stacks by standard algorithms [69], and for each particle the local bond order parameters \bar{q}_4 and \bar{q}_6 [32,70] are calculated (Fig. 4). The distribution of \bar{q}_6 and \bar{q}_4 values indicates three populations which can also be identified in the histogram of \bar{q}_6 (Fig. 4, right). The \bar{q}_6 values hence can be used to guide the classification of the particles [70]. Particles with $\bar{q}_6 \leq 0.19$ are likely to belong to the fluid, particles with $0.19 < \bar{q}_6 < 0.28$ to the bcc crystal, and particles with $\bar{q}_6 \geq 0.28$ to the fcc crystal. A similar assignment is obtained based on the number of neighbors instead of the local bond order parameter \bar{q}_6 . If the particles are labeled accordingly, the groove and interface separating the fcc and bcc crystals are clearly visible (Fig. 5, bottom). Furthermore, the orientations of the fcc and bcc bulk crystals can be determined; in both cases the (111) plane is oriented horizontally. This analysis also confirms the presence of the triple junction at the intersection of the fcc-fluid, bcc-fluid, and fcc-bcc interfaces (Figs. 3 and 5). While the three phases can be distinguished on a mesoscopic level, this is not the case on a microscopic level; individual particles are observed to

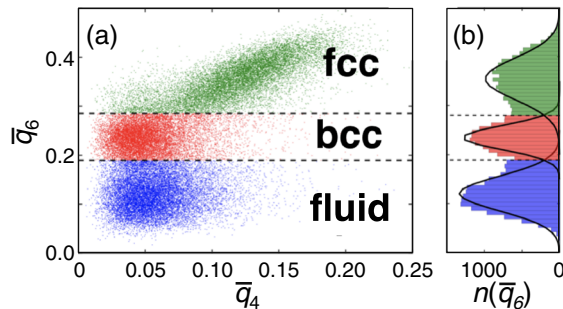


FIG. 4. (a) Local bond order parameters \bar{q}_4 and \bar{q}_6 of each particle represented by a point in the \bar{q}_4 - \bar{q}_6 plane and (b) frequency of the \bar{q}_6 values. The colors indicate the different particle properties: fcc (green), bcc (red), and fluid (blue).

spread into the neighboring regions (Fig. 5, top). Fluid particles significantly penetrate into the two crystalline regions, in particular, into the interfaces and the bcc crystal. Moreover, individual particles with bcc structure are found in the fcc and fluid regions. In contrast, the fcc particles are essentially confined to the fcc crystal with only very few particles with an fcc-like structure inside the bcc crystal. This distribution of particles is attributed to defects and fluctuations and partially could be due to the ambiguity in the link between crystal structure and \bar{q}_6 value, but also the difficulty to assign a crystal symmetry to an individual particle at finite temperature. Furthermore, the fcc-fluid interface shows a high degree of bcc-like ordering, as predicted by simulations [71].

To determine the solid-solid, i.e., fcc-bcc, interfacial energy $\gamma_{\text{fcc-bcc}}$, the groove is quantitatively analyzed. The rendered three-dimensional stack is divided into 25 quasi-two-dimensional x - y planes with a thickness of about $2.2 \mu\text{m}$ [Fig. 6(a)]. These planes are essentially parallel to the crystal planes and represent one particle layer (Fig. 5, bottom). They show grooves with slightly different depths [Fig. 6(b)].

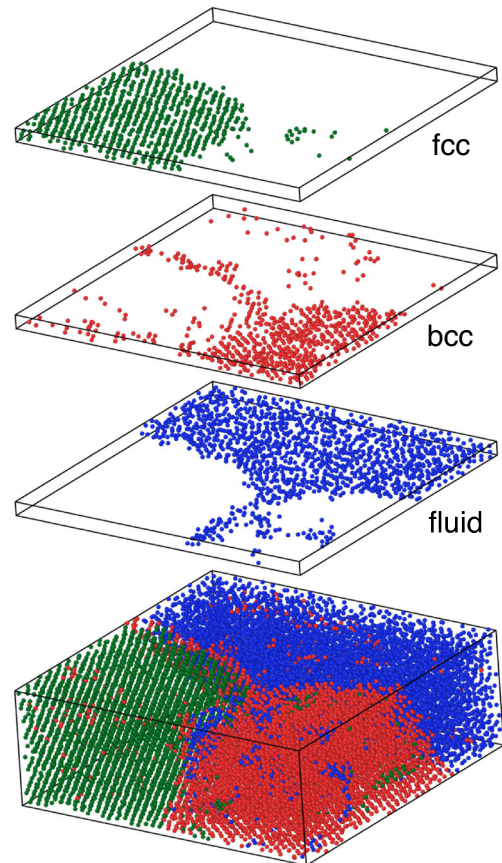


FIG. 5. Bottom: Slab of the sample ($125 \times 125 \times 45 \mu\text{m}^3$) as well as (top) the individual populations in a slice of the slab ($125 \times 125 \times 5.4 \mu\text{m}^3$) with each particle represented by a point whose color indicates the structure of the particle: fcc (green), bcc (red), and fluid (blue).

The tip of a groove, i.e., the triple junction, is defined as the particle that is most distant from the bulk fluid but still connected to the bulk fluid through other fluid particles. The structural parameters of the grooves [Fig. 1(b)] are quantitatively determined for each plane [Figs. 6(c) and 6(d)]. The grooves are slightly more than $100 \mu\text{m}$ wide and about $80 \mu\text{m}$ deep, which corresponds to about 50 particle diameters or 35 interlayer spacings. Towards the fcc crystal the depth of the groove, on average $h_{\text{fcc}} \approx 84 \mu\text{m}$, is slightly larger than towards the bcc crystal, on average $h_{\text{bcc}} \approx 72 \mu\text{m}$. We find similarly for the angles; $\beta_{\text{fcc}} \approx 8.2^\circ$ is slightly larger than $\beta_{\text{bcc}} \approx 4.9^\circ$, but both are very small. This results in a small dihedral angle $\beta = \beta_{\text{bcc}} + \beta_{\text{fcc}} \approx 13^\circ$. This is in contrast to findings for grain boundaries between crystallites with the same symmetry where the dihedral angles are larger, about 100° [48].

Mechanical stability of the triple junction line requires Young's condition to hold [68,72–74]. It links the interfacial free energies γ to the interface intersection angles β (Fig. 1):

$$\gamma_{\text{fcc-bcc}} = \gamma_{\text{fcc}} \cos(\beta_{\text{fcc}}) + \gamma_{\text{bcc}} \cos(\beta_{\text{bcc}}), \quad (1)$$

where the subscripts fcc, bcc, and fcc-bcc refer to the fcc-fluid, bcc-fluid, and fcc-bcc interfaces with $\gamma_{\text{bcc}} \approx 0.12 k_B T/a^2$ and $\gamma_{\text{fcc}} \approx 0.40 k_B T/a^2$ [44] with an extended comparison of experimental and theoretical values provided by Ref. [43]. The angles refer to the directions of the interfaces close to the triple junction. This equation is based on the assumption that the interfacial energy is isotropic. It was shown to adequately describe the fluid-bcc interfaces in Yukawa systems close to the triple conditions, where the interfacial energy is almost isotropic [44]. In addition, the

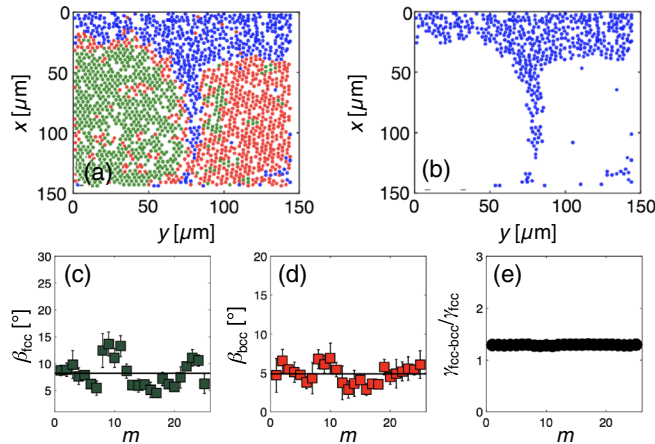


FIG. 6. (a) Particle layer with the colors of the particles indicating the corresponding phase: fcc (green), bcc (red), and fluid (blue). (b) Only the fluid particles in the same layer. (c) Angles of the groove towards the fcc crystal, β_{fcc} , and (d) towards the bcc crystal, β_{bcc} [Fig. 1(b)], as well as the (e) fcc-bcc interfacial energy $\gamma_{\text{fcc-bcc}}$, all as a function of the particle layer m .

fluid-fcc interface energy in hard sphere systems has been found to show only a modest dependence on the orientation [75]. Since the fcc-bcc interface has a fluidlike structure with many defects, it appears reasonable to assume that its interfacial energy is not very anisotropic.

Using Young's equation [Eq. (1)], the fcc-bcc, i.e., solid-solid, interfacial energy $\gamma_{\text{fcc-bcc}}$ can be calculated. We find $\gamma_{\text{fcc-bcc}} \approx 0.52 k_B T/a^2 = 1.3\gamma_{\text{fcc}}$ [Fig. 6(e)]. Thus, the interfacial energy is very small, although it involves two solid phases. The small interfacial energy is consistent with the pronounced fluctuations observed at the fcc-bcc interface (Fig. 5); the interface is several layers wide and hence astonishingly broad. The value of the interfacial energy is considered to be reliable as it shows only a very weak sensitivity to uncertainties in the angles β_{fcc} and β_{bcc} due to the small size of the angles and the dependence of $\gamma_{\text{fcc-bcc}}$ on the cosine of the angles, which is close to 1. Thus, the uncertainty in $\gamma_{\text{fcc-bcc}}$ is mainly related to the definition of the tip of the groove and less to the uncertainties in the determination of the angles β_{fcc} and β_{bcc} . Nevertheless, also the definition of the tip is not crucial, as argued in the following.

The observed coexistence of the three phases (Fig. 3) implies that none of the three interfacial energies dominates. For example, the sum of the two interfacial energies, γ_{fcc} and γ_{bcc} , represents the maximum value of $\gamma_{\text{fcc-bcc}}$ that is still compatible with the existence of a fcc-bcc interface. For larger values, the fcc-bcc interface would be unstable towards an intervening fluid phase, i.e., complete wetting. Therefore, $\gamma_{\text{fcc-bcc}} < \gamma_{\text{fcc}} + \gamma_{\text{bcc}}$ and, following the corresponding argument, $\gamma_{\text{fcc}} < \gamma_{\text{fcc-bcc}} + \gamma_{\text{bcc}}$. This implies $\gamma_{\text{fcc}} - \gamma_{\text{bcc}} < \gamma_{\text{fcc-bcc}} < \gamma_{\text{fcc}} + \gamma_{\text{bcc}}$ and hence $0.7 \lesssim \gamma_{\text{fcc-bcc}}/\gamma_{\text{fcc}} \lesssim 1.3$. This range is so narrow because the bcc-fluid interfacial energy is small, $\gamma_{\text{bcc}} \approx 0.3\gamma_{\text{fcc}}$ [44], which has been attributed to the fact that the bcc structure is relatively close to the fluid structure [44]. This narrow range of values for $\gamma_{\text{fcc-bcc}}$ hence can be established only based on the observation of the coexistence of the three phases. Moreover, the observation of a tight groove (Fig. 3) implies small angles β_{fcc} and β_{bcc} whose cosines are about 1. Thus, $\gamma_{\text{fcc-bcc}}$ is almost the sum of the two solid-fluid interfacial energies, $\gamma_{\text{fcc-bcc}} \approx \gamma_{\text{fcc}} + \gamma_{\text{bcc}} \approx 1.3\gamma_{\text{fcc}}$ [Eq. (1)]. The value of $\gamma_{\text{fcc-bcc}}$ hence is expected towards the upper limit of the above range of values. This semiquantitative argument is based on the observation of individual particles. However, it does not require us to define the tip of the groove; the observation of a tight groove is sufficient. Thus, there is qualitative support as well as semiquantitative and quantitative evidence for a very small fcc-bcc interfacial energy.

To conclude, we investigated suspensions of charged colloids under triple conditions, where a fcc crystal, a bcc crystal, and a fluid coexist. The fcc-bcc interfacial energy was found to be about 1.3 times higher than the fcc-fluid interfacial energy close to the triple point with $\gamma_{\text{fcc-bcc}} \approx 0.52 k_B T/a^2$. Thus, the fcc-bcc interfacial energy

is very small, despite the fact that two solid phases are involved. This is consistent with the observation of broad interfaces and indicates the importance of thermal fluctuations also for solid-solid interfaces. Our quantitative findings and qualitative arguments suggest that a small solid-solid interfacial energy not only occurs in systems with charged particles but also in other systems with soft interactions exhibiting a triple point. Furthermore, also in atomic or molecular systems, e.g., metals [76–79], similar values might be found if expressed in dimensionless units. Our finding hence might in general apply to triple points involving a fluid and two solids. They might also be extended to more complex conditions, such as the presence of shear or other external fields [80–82].

We thank F. Spaepen, A. G. Yodh, and T. Palberg for very useful discussions and P. Maßhoff for help with the figures. M. C. is supported by a Marie-Curie international outgoing fellowship within the European Union’s 7th Framework Program (Grant No. 327168). We acknowledge support by the Deutsche Forschungsgemeinschaft (Grants No. AL2058/1-1, No. LO418/19-1, and No. EG268/6-1). Part of this work was supported by the Harvard MRSEC (DMR-1420570) and NSF (DMR-1310266), and used the experimental facilities at Centre for Nanoscale Systems (CNS), a member of the National Nanotechnology Infrastructure Network (NNIN), which is supported by the National Science Foundation (ECS-0335765).

*Corresponding author.

stefan.egelhaaf@uni-duesseldorf.de

- [1] H. B. Callen, *Thermodynamics and an Introduction to Thermostatistics* (John Wiley & Sons, New York, 1985).
- [2] J. C. Heyraud and J. J. Metois, Equilibrium shape and temperature—Lead on graphite, *Surf. Sci.* **128**, 334 (1983).
- [3] H. Löwen, Equilibrium shapes of crystals near the triple point, *Surf. Sci.* **234**, 315 (1990).
- [4] S. M. Ilett, A. Orrock, W. C. K. Poon, and P. N. Pusey, Phase behavior of a model colloid-polymer mixture, *Phys. Rev. E* **51**, 1344 (1995).
- [5] W. C. K. Poon, F. Renth, R. M. L. Evans, D. J. Fairhurst, M. E. Cates, and P. N. Pusey, Colloid-Polymer Mixtures at Triple Coexistence: Kinetic Maps from Free-Energy Landscapes, *Phys. Rev. Lett.* **83**, 1239 (1999).
- [6] V. J. Anderson and H. N. W. Lekkerkerker, Insight into phase transition kinetics from colloidal science, *Nature (London)* **416**, 811 (2002).
- [7] C. P. Royall, M. E. Leunissen, A.-P. Hynninen, M. Dijkstra, and A. van Blaaderen, Re-entrant melting and freezing in a model system of charged colloids, *J. Chem. Phys.* **124**, 244706 (2006).
- [8] A. Ivlev, H. Löwen, G. Morfill, and C. P. Royall, *Complex Plasmas and Colloidal Dispersions: Particle-Resolved Studies of Classical Liquids and Solids* (World Scientific, Singapore, 2012).
- [9] E. B. Sirota, H. D. Ou-Yang, S. K. Sinha, P. M. Chaikin, J. D. Axe, and Y. Fujii, Complete Phase Diagram of a Charged Colloidal System: A Synchrotron X-Ray Scattering Study, *Phys. Rev. Lett.* **62**, 1524 (1989).
- [10] Y. Monovoukas and A. P. Gast, The experimental phase diagram of charged colloidal suspensions, *J. Colloid Interface Sci.* **128**, 533 (1989).
- [11] A.-P. Hynninen and M. Dijkstra, Phase diagrams of hard-core repulsive Yukawa particles, *Phys. Rev. E* **68**, 021407 (2003).
- [12] G. Dupont, S. Moulinasse, J. P. Ryckaert, and M. Baus, The b.c.c.-f.c.c.-fluid triple point as obtained from Monte Carlo simulations of the Yukawa model for mono-disperse colloidal suspensions, *Mol. Phys.* **79**, 453 (1993).
- [13] S. Hamaguchi, R. T. Farouki, and D. H. E. Dubin, Triple point of Yukawa systems, *Phys. Rev. E* **56**, 4671 (1997).
- [14] E. J. Meijer and D. Frenkel, Melting line of Yukawa system by computer simulation, *J. Chem. Phys.* **94**, 2269 (1991).
- [15] M. J. Stevens and M. O. Robbins, Melting of Yukawa systems: A test of phenomenological melting criteria, *J. Chem. Phys.* **98**, 2319 (1993).
- [16] Y. Peng, Z.-R. Wang, A. M. Alsayed, A. G. Yodh, and Y. Han, Melting of Colloidal Crystal Films, *Phys. Rev. Lett.* **104**, 205703 (2010).
- [17] M. Watzlawek, C. N. Likos, and H. Löwen, Phase Diagram of Star Polymer Solutions, *Phys. Rev. Lett.* **82**, 5289 (1999).
- [18] D. Gottwald, C. N. Likos, G. Kahl, and H. Löwen, Phase Behavior of Ionic Microgels, *Phys. Rev. Lett.* **92**, 068301 (2004).
- [19] H. M. Thomas and G. E. Morfill, Melting dynamics of a plasma crystal, *Nature (London)* **379**, 806 (1996).
- [20] G. E. Morfill and A. V. Ivlev, Complex plasmas: An interdisciplinary research field, *Rev. Mod. Phys.* **81**, 1353 (2009).
- [21] J. H. Chu and Lin I, Direct Observation of Coulomb Crystals and Liquids in Strongly Coupled rf Dusty Plasmas, *Phys. Rev. Lett.* **72**, 4009 (1994).
- [22] V. E. Fortov, A. V. Ivlev, S. A. Khrapak, A. G. Khrapak, and G. E. Morfill, Complex (dusty) plasmas: Current status, open issues, perspectives, *Phys. Rep.* **421**, 1 (2005).
- [23] O. S. Vaulina and S. A. Khrapak, Scaling law for the fluid-solid phase transition in Yukawa systems (dusty plasmas), *J. Exp. Theor. Phys.* **90**, 287 (2000).
- [24] U. Gasser, E. R. Weeks, A. Schofield, P. N. Pusey, and D. A. Weitz, Real-space imaging of nucleation and growth in colloidal crystallization, *Science* **292**, 258 (2001).
- [25] P. Wette, H. J. Schöpe, and T. Palberg, Microscopic investigations of homogeneous nucleation in charged sphere suspensions, *J. Chem. Phys.* **123**, 174902 (2005).
- [26] T. Kawasaki and H. Tanaka, Formation of a crystal nucleus from liquid, *Proc. Natl. Acad. Sci. U.S.A.* **107**, 14036 (2010).
- [27] Z. R. Wang, F. Wang, Y. Peng, Z. Y. Zheng, and Y. L. Han, Imaging the homogenous nucleation during the melting of superheated colloidal crystals, *Science* **338**, 87 (2012).
- [28] E. Zaccarelli, C. Valeriani, E. Sanz, W. C. K. Poon, M. Cates, and P. N. Pusey, Crystallization of Hard-Sphere Glasses, *Phys. Rev. Lett.* **103**, 135704 (2009).
- [29] H. Zhou, S. Xu, Z. Sun, X. Du, and L. Liu, Kinetics study of crystallization with the disorder-bcc-fcc phase transition of charged colloidal dispersions, *Langmuir* **27**, 7439 (2011).

- [30] A. G. Shabalin, J.-M. Meijer, R. Dronyak, O. M. Yefanov, A. Singer, R. P. Kurta, U. Lorenz, O. Y. Gorobtsov, D. Dzhibaev, S. Kalbfleisch, J. Gulden, A. V. Zozulya, M. Sprung, A. V. Petukhov, and I. A. Vartanyants, Revealing Three-Dimensional Structure of an Individual Colloidal Crystal Grain by Coherent X-Ray Diffractive Imaging, *Phys. Rev. Lett.* **117**, 138002 (2016).
- [31] T. Schilling, H. J. Schöpe, M. Oettel, G. Opletal, and I. Snook, Precursor-Mediated Crystallization Process in Suspensions of Hard Spheres, *Phys. Rev. Lett.* **105**, 025701 (2010).
- [32] E. Allahyarov, K. Sandomirski, S. U. Egelhaaf, and H. Löwen, Crystallization seeds favour crystallization only during initial growth, *Nat. Commun.* **6**, 7110 (2015).
- [33] N. Lorenz and T. Palberg, Melting and freezing lines for a mixture of charged colloidal spheres with spindle type phase diagram, *J. Chem. Phys.* **133**, 104501 (2010).
- [34] J. Sprakel, A. Zaccone, F. Spaepen, P. Schall, and D. A. Weitz, Direct Observation of Entropic Stabilization of bcc Crystals Near Melting, *Phys. Rev. Lett.* **118**, 088003 (2017).
- [35] J. Loehr, A. Ortiz-Ambriz, and P. Tierno, Defect Dynamics in Artificial Colloidal Ice: Real-Time Observation, Manipulation, and Logic Gate, *Phys. Rev. Lett.* **117**, 168001 (2016).
- [36] E. R. Weeks, J. C. Crocker, A. C. Levitt, A. Schofield, and D. A. Weitz, Three-dimensional direct imaging of structural relaxation near the colloidal glass transition, *Science* **287**, 627 (2000).
- [37] H. Tanaka, T. Kawasaki, H. Shintani, and K. Watanabe, Critical-like behaviour of glass-forming liquids, *Nat. Mater.* **9**, 324 (2010).
- [38] M. Leocmach and H. Tanaka, Roles of icosahedral and crystal-like order in the hard spheres glass transition, *Nat. Commun.* **3**, 974 (2012).
- [39] B. Zhang and X. Cheng, Structures and Dynamics of Glass-Forming Colloidal Liquids under Spherical Confinement, *Phys. Rev. Lett.* **116**, 098302 (2016).
- [40] J. Hernandez-Guzman and E. Weeks, The equilibrium intrinsic crystal-liquid interface of colloids, *Proc. Natl. Acad. Sci. U.S.A.* **106**, 15198 (2009).
- [41] I. B. Ramsteiner, D. A. Weitz, and F. Spaepen, Stiffness of the crystal-liquid interface in a hard-sphere colloidal system measured from capillary fluctuations, *Phys. Rev. E* **82**, 041603 (2010).
- [42] V. D. Nguyen, M. T. Dang, B. Weber, Z. Hu, and P. Schall, Visualizing the structural solid-liquid transition at colloidal crystal/fluid interfaces, *Adv. Mater.* **23**, 2716 (2011).
- [43] T. Palberg, P. Wette, and D. M. Herlach, Equilibrium fluid-crystal interfacial free energy of bcc-crystallizing aqueous suspensions of polydisperse charged spheres, *Phys. Rev. E* **93**, 022601 (2016).
- [44] V. Heinonen, A. Mijailovic, C. V. Achim, T. Ala-Nissila, R. E. Rozas, J. Horbach, and H. Löwen, Bcc crystal-fluid interfacial free energy in Yukawa systems, *J. Chem. Phys.* **138**, 044705 (2013).
- [45] A. Yethiraj, A. Wouterse, B. Groh, and A. van Blaaderen, Nature of an Electric-Field-Induced Colloidal Martensitic Transition, *Phys. Rev. Lett.* **92**, 058301 (2004).
- [46] M. T. Casey, R. T. Scarlett, W. B. Rogers, I. Jenkins, T. Sinno, and J. C. Crocker, Driving diffusionless transformations in colloidal crystals using DNA handshaking, *Nat. Commun.* **3**, 1209 (2012).
- [47] Y. Peng, F. Wang, Z. Wang, A. M. Alsayed, Z. Zhang, A. G. Yodh, and Y. Han, Two-step nucleation mechanism in solid-solid phase transitions, *Nat. Mater.* **14**, 101 (2015).
- [48] E. Maire, E. Redston, M. P. Gulda, D. A. Weitz, and F. Spaepen, Imaging grain boundary grooves in hard-sphere colloidal bicrystals, *Phys. Rev. E* **94**, 042604 (2016).
- [49] F. Evers, R. D. L. Hanes, C. Zunke, R. F. Capellmann, J. Bewerunge, C. Dalle-Ferrier, M. C. Jenkins, I. Ladadwa, A. Heuer, R. Castaneda-Priego, and S. U. Egelhaaf, Colloids in Light Fields: Particle Dynamics in Random and Periodic Energy Landscapes, *Eur. Phys. J. Spec. Top.* **222**, 2995 (2013).
- [50] M. Laurati, P. Maßhoff, K. J. Mutch, S. U. Egelhaaf, and A. Zaccone, Long-Lived Neighbors Determine the Rheological Response of Glasses, *Phys. Rev. Lett.* **118**, 018002 (2017).
- [51] T. Sentjabrskaja, P. Chaudhuri, M. Hermes, W. C. K. Poon, J. Horbach, S. U. Egelhaaf, and M. Laurati, Creep and flow of glasses: Strain response linked to the spatial distribution of dynamical heterogeneities, *Sci. Rep.* **5**, 11884 (2015).
- [52] P. Schall, D. A. Weitz, and F. Spaepen, Structural rearrangements that govern flow in colloidal glasses, *Science* **318**, 1895 (2007).
- [53] A. Yethiraj and A. van Blaaderen, A colloidal model system with an interaction tunable from hard sphere to soft and dipolar, *Nature (London)* **421**, 513 (2003).
- [54] A. Yethiraj, Tunable colloids: Control of colloidal phase transitions with tunable interactions, *Soft Matter* **3**, 1099 (2007).
- [55] F. Hsu, E. R. Dufresne, and D. A. Weitz, Charge stabilization in nonpolar solvents, *Langmuir* **21**, 4881 (2005).
- [56] K. Mukherjee, S. P. Mouli, and D. C. Mukherjee, Thermodynamics of micellization of aerosol OT in polar and nonpolar solvents. A calorimetric study, *Langmuir* **9**, 1727 (1993).
- [57] T. Kanai, N. Boon, P. J. Lu, E. Sloutskin, A. B. Schofield, F. Smallenburg, R. van Roij, M. Dijkstra, and D. A. Weitz, Crystallization and reentrant melting of charged colloids in nonpolar solvents, *Phys. Rev. E* **91**, 030301 (2015).
- [58] M. Zulauf and H.-F. Eicke, Inverted micelles and microemulsions in the ternary system water/aerosol-OT/isoctane as studied by photon correlation spectroscopy, *J. Phys. Chem.* **83**, 480 (1979).
- [59] E. J. W. Verwey and J. T. G. Overbeek, *Theory of the Stability of Lyophobic Colloids* (Elsevier, Amsterdam, 1948).
- [60] L. Bocquet, E. Trizac, and M. Aubouy, Effective charge saturation in colloidal suspensions, *J. Chem. Phys.* **117**, 8138 (2002).
- [61] The samples are filled in glass capillaries with a size of about $15 \times 5 \times 0.2 \text{ mm}^3$ and left for 2 days to allow for equilibration before volumes of $145 \times 145 \times 60 \text{ }\mu\text{m}^3$, corresponding to $512 \times 512 \times 478$ voxels, and located $20 \text{ }\mu\text{m}$ from the capillary wall are imaged using a confocal microscope (Leica TCS SP5 with a $40\times$ oil-immersion objective).

- [62] S. Hamaguchi, R. T. Farouki, and D. H. E. Dubin, Phase diagram of Yukawa systems near the one-component-plasma limit revisited, *J. Chem. Phys.* **105**, 7641 (1996).
- [63] K. Kremer, M. O. Robbins, and G. S. Grest, Phase Diagram of Yukawa Systems: Model for Charge-Stabilized Colloids, *Phys. Rev. Lett.* **57**, 2694 (1986).
- [64] S. Sengupta and A. K. Sood, Theory of liquid-bcc-fcc coexistence in charge-stabilized colloidal systems, *Phys. Rev. A* **44**, 1233 (1991).
- [65] F. Smallenburg, N. Boon, M. Kater, M. Dijkstra, and R. van Roij, Phase diagram of colloidal spheres with constant zeta-potential, *J. Chem. Phys.* **134**, 074505 (2011).
- [66] H. J. Schöpe, T. Decker, and T. Palberg, Response of the elastic properties of colloidal crystals to phase transitions and morphological changes, *J. Chem. Phys.* **109**, 10068 (1998).
- [67] I. R. de Anda, A. Statt, F. Turci, and C. P. Royall, Low-density crystals in charged colloids: Comparison with Yukawa theory, *Contrib. Plasma Phys.* **55**, 172 (2015).
- [68] R. B. Rogers and B. J. Ackerson, The measurement of solid-liquid interfacial energy in colloidal suspensions using grain boundary grooves, *Philos. Mag.* **91**, 682 (2011).
- [69] J. C. Crocker and D. G. Grier, Methods of digital video microscopy for colloidal studies, *J. Colloid Interface Sci.* **179**, 298 (1996).
- [70] P. R. ten Wolde, M. J. Ruiz-Montero, and D. Frenkel, Simulation of homogeneous crystal nucleation close to coexistence, *Faraday Discuss.* **104**, 93 (1996).
- [71] P. R. ten Wolde, M. J. Ruiz-Montero, and D. Frenkel, Numerical Evidence for bcc Ordering at the Surface of a Critical fcc Nucleus, *Phys. Rev. Lett.* **75**, 2714 (1995).
- [72] W. W. Mullins, Theory of thermal grooving, *J. Appl. Phys.* **28**, 333 (1957).
- [73] H. J. Vogel and L. Ratke, Instability of grain boundary grooves due to equilibrium grain boundary diffusion, *Acta Metall. Mater.* **39**, 641 (1991).
- [74] S.-C. Lin, M.-W. Liu, M. P. Gururajan, and K.-A. Wu, Modified Young's equation for equilibrium dihedral angles of grain boundary grooves in thin films at the nanoscale, *Acta Mater.* **102**, 364 (2016).
- [75] A. Härtel, M. Oettel, R. E. Rozas, S. U. Egelhaaf, J. Horbach, and H. Löwen, Tension and Stiffness of the Hard Sphere Crystal-Fluid Interface, *Phys. Rev. Lett.* **108**, 226101 (2012).
- [76] M. Hillert, *Phase Equilibria, Phase Diagrams and Phase Transformations: Their Thermodynamic Basis* (Cambridge University Press, Cambridge, England, 1998).
- [77] G. I. Tóth, G. Tegze, T. Pusztai, G. Tóth, and L. Gránásy, Polymorphism, crystal nucleation and growth in the phase-field crystal model in 2D and 3D, *J. Phys. Condens. Matter* **22**, 364101 (2010).
- [78] H. Emmerich, Nucleation and growth kinetics in colloids and metals: A system- and scale-bridging approach to understanding the resulting morphology evolution, *Philos. Mag. Lett.* **87**, 795 (2007).
- [79] G. C. Sosso, J. Chen, S. J. Cox, M. Fitzner, P. Pedevilla, A. Zen, and A. Michaelides, Crystal nucleation in liquids: Open questions and future challenges in molecular dynamics simulations, *Chem. Rev.* **116**, 7078 (2016).
- [80] J. K. G. Dhont, Shear Induced Displacement of the Spinodal of Brownian Systems, *Phys. Rev. Lett.* **76**, 4269 (1996).
- [81] M. P. Lettinga, H. Wang, and J. K. G. Dhont, Microstructural response of a near-critical colloid-polymer mixture to shear flow, *Phys. Rev. E* **70**, 061405 (2004).
- [82] C. Bechinger, M. Brunner, and P. Leiderer, Phase Behavior of Two-Dimensional Colloidal Systems in the Presence of Periodic Light Fields, *Phys. Rev. Lett.* **86**, 930 (2001).